

Unified Mapmaking for Anisotropic Stochastic Gravitational Wave Background

Jishnu Suresh*

Institute for Cosmic Ray Research (ICRR), The University of Tokyo, Kashiwa City, Chiba 277-8582, Japan

Anirban Ain†

Istituto Nazionale di Fisica Nucleare sez. Pisa, 56126 Pisa, Italy

Sanjit Mitra‡

Inter-University Centre for Astronomy and Astrophysics (IUCAA), Pune 411007, India

A stochastic gravitational wave background (SGWB), created by the superposition of signals from unresolved astrophysical sources, may be detected in the next few years. Several theoretical predictions are being made about the possible nature of anisotropies in the background. Estimating and mapping the intensity across the sky can therefore play a key role in improving our understanding of astrophysical models. Skymaps have been produced in the pixel and spherical harmonic basis for all the data taking runs of the advanced ground-based interferometric detectors. While these maps are being produced with similar algorithms, the underlying algebra and numerical implementations remain different. Which is why there was a need for producing results in both bases. We show that these manifestly redundant methods could be unified to a single analysis in practice as well. We first develop the algebra to show that the results, maps, and noise covariance matrices, in two different bases are easily transformable. We then incorporate both schemes, in the now standard analysis pipeline for anisotropic SGWB, `PyStoch`. We then show that the transformed results in the pixel and spherical harmonic bases match very well. Thus concluding that a single skymap will be sufficient to describe the anisotropies in a stochastic background. The multiple capabilities of `PyStoch` will be useful for estimating various measures to characterise an anisotropic background.

I. INTRODUCTION

A new era of astronomy began with the detection of gravitational waves (GW) [1] by the Advanced Laser Interferometric Gravitational-wave Observatory (LIGO), followed by tens of binary mergers [2]. These detections have opened up new avenues for exploring the late and early stages of the universe. A vigorous global effort is underway to observe GW signals in widely separated frequency bands. Current and future networks of detectors have the potential to detect not only astrophysical sources but also sources of cosmological origin. Among these sources, the stochastic gravitational wave background (SGWB) [3, 4] is one of the most interesting ones. A large number of unresolved distant compact binary coalescences [5] and millisecond pulsars in galaxy clusters [6–9] can produce an astrophysical background, which are close to the sensitivity levels of the current or upcoming ground-based interferometers. The background can be significantly anisotropic due to the non-uniform distribution of astrophysical sources in the local universe [10]. Based on the recent rate estimation from the observed GW signals [5] and the pulsar timing array data [11, 12], the detection of SGWB seems promising in the near future.

Several methods [4, 13–18] have been proposed in the past to estimate the intensity variation of a SGWB

across the sky. This procedure of obtaining the spatial distribution of intensity—the skymap—is often referred to as the map-making process. The standard algorithms have been thoroughly investigated and implemented in the pixel [19, 20] as well as in the spherical harmonic basis [21]. Alternative approaches for the spherical harmonic basis have also been proposed Allen and Ottewill [4], Renzini and Contaldi [22]. The spherical harmonic basis is appropriate for smooth and diffuse sources whereas the pixel basis is suited for localised point-like sources. The efficiency of these “radiometer” algorithms was dramatically improved through the mechanism of data folding [23]. Recently, we developed a new pipeline called `PyStoch` [24], which can boost the efficiency of the map-making process by another factor of few tens. `PyStoch` is the first implementation of a radiometer search that is fully integrated with the Hierarchical Equal Area isoLatitude Pixelization of a sphere `HEALPix` [25] scheme. `HEALPix` offers highly efficient tools for Fourier transforms on the sky, and other methods useful for skymap analysis and manipulation. Other than the speed improvement in the analysis, we designed the pipeline in a way that the intermediate results, the skymaps at each frequency bin (narrowband maps), combining data from multiple detectors can all be done straightforwardly in an integrated way.

Here we report on the extension of the `PyStoch` pipeline to search for broad sources in the spherical harmonic basis, thereby making `PyStoch` the one single code to perform all the current SGWB anisotropy analyses in an efficient way. We discuss how we implement the spherical harmonic decomposition algorithm in `PyStoch`

* jishnu@icrr.u-tokyo.ac.jp

† anirban.ain@pi.infn.it

‡ sanjit@iucaa.in

starting from the pixel based results. With this unified map-making pipeline, a separate search pipeline for anisotropic SGWB in a spherical harmonic domain becomes redundant.

This paper is organized as follows: Sec. II briefly reviews the GW radiometer algebra and provides a detailed description of the analysis in the spherical harmonic basis. In Sec. III, we discuss the implementation of the new method in the existing **PyStoch** pipeline and show that the transformed results in pixel and spherical harmonic basis match very well. In Sec. IV, we discuss the implications of our result and its immediate advantages for SGWB searches.

II. METHOD

An SGWB is estimated from the cross-power spectral density (CSD) of data from pairs of detectors [13]. Assuming the SGWB frequency spectral shape to be $H(f)$ and that it is the same in every direction on the sky, a search for a specific spectral distribution boils down to estimation of the SGWB skymap $\mathcal{P}(\hat{\Omega})$. The “skymap” $\mathcal{P}(\hat{\Omega})$ is proportional to the flux coming from different directions on the sky [20]. One can perform the search in any set of basis $e(\hat{\Omega})$ on the two-sphere [21], in which the anisotropy map can be expanded as,

$$\mathcal{P}(\hat{\Omega}) := \sum_p \mathcal{P}_p e_p(\hat{\Omega}). \quad (1)$$

The maximum-likelihood (ML) method for mapping this GW intensity have been implemented in two natural basis, the pixel basis [19, 20] and the spherical harmonic (SpH) basis [21]. Even though the search should determine the choice of basis, earlier analyses were forced to choose the SpH basis for most part [26, 27], due to severe limitations in computation, in both cost and numerical accuracy, especially in dealing with large Fisher matrices in pixel basis. Recently the introduction of **PyStoch** with folded data has made the searches very efficient, which allows us to choose the basis freely eliminating computational limitations. Initially **PyStoch** was written for the pixel basis. Here we show how we enhance **PyStoch** by adding the capability to perform SpH search, unifying the approaches for the two bases.

In the pixel basis, which is appropriate to search for an anisotropic SGWB dominated by a localised point-like source, one can decompose the angular power distribution from Eq. (1) as,

$$\mathcal{P}(\hat{\Omega}) = \mathcal{P}_{\hat{\Omega}'} \delta(\hat{\Omega}, \hat{\Omega}'). \quad (2)$$

In contrast, the SpH basis is suitable to search for a diffuse background which may be dominated by say a dipolar or a quadrupolar distribution. We can expand the anisotropy map over the basis functions Y_{lm} as,

$$\mathcal{P}(\hat{\Omega}) = \sum_{lm} \mathcal{P}_{lm} Y_{lm}(\hat{\Omega}). \quad (3)$$

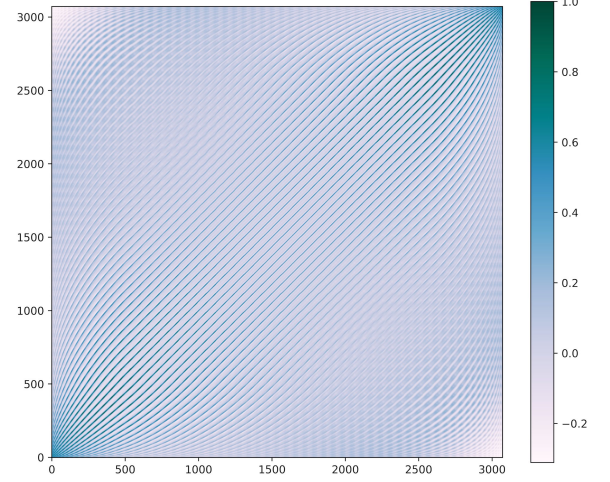


FIG. 1. A characteristic beam matrix for the LIGO Hanford-Livingston baseline at $\sim 3^\circ$ pixel size (**HEALPix**^a $n_{\text{side}} = 16$). Each row of the matrix is the antenna response function for the pointing direction. Since the GW radiometer receives maximum contribution from the pointing direction, this matrix is dominated by the diagonal elements. Here the stripes are related to the isoLatitude pixelization scheme.

^a <http://healpix.sf.net>

Here we follow $Y_{lm}(\theta, \phi)$ conventions used in Jackson [28]. A standard ML solution for $\hat{\mathcal{P}}(\hat{\Omega})$ in a general basis, which produces the estimates for the SGWB skymaps, can be obtained using the existing methods as [20, 21, 24],

$$\hat{\mathcal{P}}_{\hat{\Omega}} \equiv \hat{\mathcal{P}} = \mathbf{\Gamma}^{-1} \cdot \mathbf{X}, \quad (4)$$

where $\mathbf{X} \equiv X_p$, the “dirty” map, is given as,

$$X_p = \frac{4}{\tau} \sum_{Ift} \frac{H(f) \gamma_{ft,p}^{I*}}{P_{\mathcal{I}_1}(t; f) P_{\mathcal{I}_2}(t; f)} \tilde{s}_{\mathcal{I}_1}^*(t; f) \tilde{s}_{\mathcal{I}_2}(t; f), \quad (5)$$

and $\mathbf{\Gamma} \equiv \Gamma_{pp'}$, the Fisher information matrix, as,

$$\Gamma_{pp'} = 4 \sum_{Ift} \frac{H^2(f)}{P_{\mathcal{I}_1}(t; f) P_{\mathcal{I}_2}(t; f)} \gamma_{ft,p}^{I*} \gamma_{ft,p'}^I. \quad (6)$$

$P_{\mathcal{I}_{1,2}}(t; f)$ are the one-sided noise power spectral density (PSD) of the individual detectors (\mathcal{I}_1 or \mathcal{I}_2) for the data segment at time t (τ represent the entire observation duration). Here $\gamma_{ft,\hat{\Omega}}^I$ is a geometric factor which accounts for the signal interference and the reduction in sensitivity due to the geometric non-alignment and geographic separation of the detectors, known as the overlap reduction

function (ORF). It is defined as [15, 29],

$$\gamma_{ft,p}^I := \sum_A \int_{S^2} d\hat{\Omega} F_{\mathcal{I}_1}^A(\hat{\Omega}, t) F_{\mathcal{I}_2}^A(\hat{\Omega}, t) e^{2\pi i f \frac{\hat{\Omega} \cdot \Delta \mathbf{x}_I(t)}{c}} e_p(\hat{\Omega}), \quad (7)$$

where $\Delta \mathbf{x}_I(t)$ is the detector separation vector. The polarizations are denoted by $A = +, \times$, and $F_{\mathcal{I}_{1,2}}^A(\hat{\Omega}, t)$ denotes the respective antenna pattern functions. Calculations of the ORF plays a crucial role in performing SGWB searches. The ORF expressed in a general basis in Eq. (7) can be converted to the desired search basis. In the pixel basis, one can write the ORF as,

$$\gamma_{ft,\hat{\Omega}}^I = \sum_A F_{\mathcal{I}_1}^A(\hat{\Omega}, t) F_{\mathcal{I}_2}^A(\hat{\Omega}, t) e^{2\pi i f \frac{\hat{\Omega} \cdot \Delta \mathbf{x}_I(t)}{c}}. \quad (8)$$

Similarly, for the spherical harmonic basis, one can write,

$$\gamma_{ft,lm}^I = \int_{S^2} d\hat{\Omega} \gamma_{ft,\hat{\Omega}}^I Y_{lm}^*(\hat{\Omega}). \quad (9)$$

Since the change in the ORF due to the rotation of the earth in time t is equivalent of increasing the azimuthal angle ϕ about the spin axis by $-2\pi t/T$, following the definition of spherical harmonics, one can write [4, 13],

$$\gamma_{ft,lm}^I = \gamma_{f0,lm}^I e^{im2\pi t/T}, \quad (10)$$

where T is the period of rotation of the earth, which is by definition one sidereal day. Thus $\gamma_{ft,lm}^I$ can be computed at all values of t , using $\gamma_{f0,lm}^I$, the spherical harmonic transform of $\gamma_{ft,\hat{\Omega}}^I$ at a fiducial $t = 0$. This step significantly reduces computation cost, by alleviating the need to perform a spherical harmonic transform of $\gamma_{ft,\hat{\Omega}}^I$ at each of the ~ 1000 segments in one sidereal day. This is particularly important for the new all-sky-all-frequency (ASAF) search, where this quantity must be computed at every frequency bin, which are few tens of thousands in number for the frequency bin size of 1/32Hz presently being used in LIGO-Virgo analyses. With the help of this technique, we have enabled **PyStoch** to perform ASAF search in the SpH basis, along with the pixel basis, which it was already capable of doing. While the spherical harmonic moments estimated through this route match those obtained directly from the pixel based map (Fig. 2), these tools will nevertheless be required for estimating statistical quantities in SpH basis and will remain useful for faster execution of (perhaps exploratory) analyses where the pixel based maps may not be necessary.

The (square) matrix Γ in Eq. (6) is usually called the Fisher information matrix. The calculation of the Fisher matrix becomes straightforward if we follow the implementation of ORF discussed above. Since **PyStoch** is able to calculate the Fisher matrix $\Gamma_{\hat{\Omega},\hat{\Omega}'}$ in the pixel basis, which can be written as

$$\Gamma_{\hat{\Omega},\hat{\Omega}'} = 4 \sum_{Ift} \frac{H^2(f)}{P_{\mathcal{I}_1}(t; f) P_{\mathcal{I}_2}(t; f)} \gamma_{ft,\hat{\Omega}}^{I*} \gamma_{ft,\hat{\Omega}'}^I. \quad (11)$$

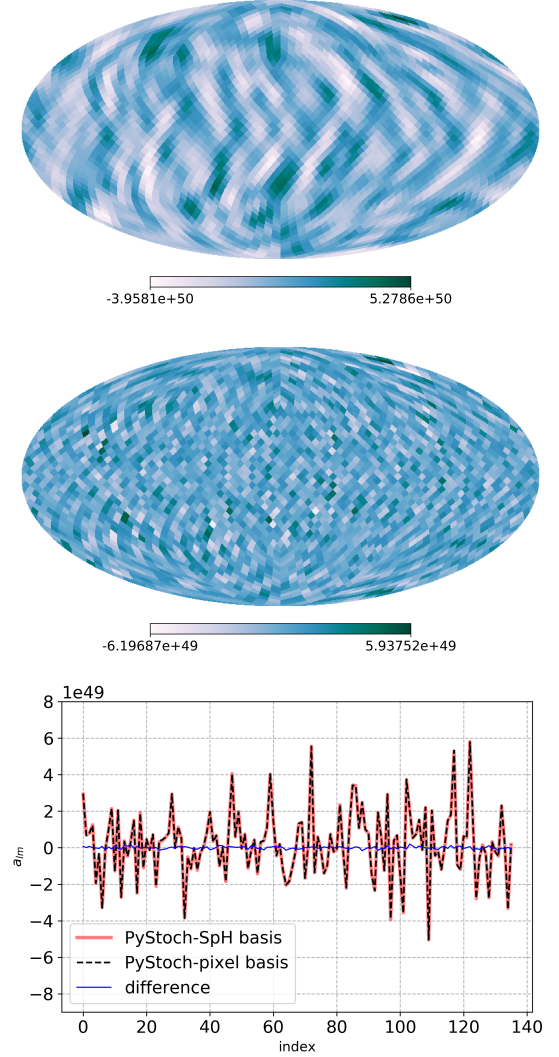


FIG. 2. Results from direct pixel to SpH transformation performed on the dirty map using **HEALPix** tool are shown here. The pixel-space broadband result from the folded data using **PyStoch** is shown on the top. The map in the middle shows the difference between the results from **PyStoch** pixel basis (top) and the map derived from the SpH coefficients. In both the skymaps, $n_{\text{side}} = 16$, power-law spectral indices $\alpha = 3$ and $l_{\text{max}} = 30$ were used. We have also compared the a_{lm} obtained from the two bases (only showed values up to $l_{\text{max}} = 15$). The fractional RMS differences are nearly 0.1%. The difference in SpH basis results obtained using **PyStoch** and the conventional pipeline are very small, less than 10^{-4} (see Fig. 4).

In the SpH basis the Fisher matrix elements are given by,

$$\Gamma_{lm,l'm'} = 4 \sum_{Ift} \frac{H^2(f)}{P_{\mathcal{I}_1}(t; f) P_{\mathcal{I}_2}(t; f)} \gamma_{ft,lm}^{I*} \gamma_{ft,l'm'}^I. \quad (12)$$

For odd values of $l + l'$ these elements vanish [21]. One can use $\gamma_{ft,lm}^I$ obtained above to compute the non-zero elements of the matrix. Note that this approach is differ-

ent from the existing method [21], however, the results match to better than one part in 10^4 in terms of Root Mean Square (RMS) difference between the dirty maps, SpH moments, and the Fisher matrices (Figs. 4 & 6). Our method, powered by Fast-Fourier Transform employed by `HEALPix`, is highly efficient and, also, due to the lack of a straightforward recipe, we have not compared the relative performances of the two approaches.

III. IMPLEMENTATION

`PyStoch` code, with the new tools, can simultaneously produce results in both spherical harmonic and pixel basis. The results have been validated using the GW data from the first observing run of LIGO Hanford-Livingston detectors. We have created the mentioned dataset by following the steps described in Ain *et al.* [23]. The dataset consists of 898 frames of CSDs and PSDs. Each with a 50% overlapping segment duration of 192 sec which spans nearly one full sidereal day. Considering the optimal resolution required for the radiometer analysis for the two LIGO detectors, we choose the `HEALPix` map resolution to be $n_{\text{side}} = 16$ ¹. This corresponds to $n_{\text{pix}} = 3072$ pixels for the entire sky, each pixel is nearly square with a width of approximately 3 degrees.

For a source whose intensity varies slowly across the sky, l_{max} could be small; on the other hand, for sources with sharply varying spatial distributions l_{max} is expected to be large. A recommended relation between pixel and SpH resolution is [25],

$$n_{\text{pix}} = 12 n_{\text{side}}^2 \approx \frac{4}{\pi} l_{\text{max}}^2. \quad (13)$$

Although the equivalent l_{max} corresponding to $n_{\text{side}} = 16$ is higher according to Eq. 13, we have used an $l_{\text{max}} = 30$ for our study.²

A. Calculating Overlap Reduction Function

`PyStoch` uses a novel technique for calculating ORF through seed matrices [24]. The time-dependent part of the ORF in Eq. (7) can be separated from the frequency-dependent part by calculating $F_{\mathcal{I}_1}^A(\hat{\Omega}, t) F_{\mathcal{I}_2}^A(\hat{\Omega}, t)$ and $\hat{\Omega} \cdot \Delta \mathbf{x}_I(t)/c$ separately as maps in the basis we are using. For a fixed time segment and baseline, these two maps are frequency-independent. We call these maps ORF seed matrices. `PyStoch` calculates and saves them for each set of data and automatically loads them for subsequent analysis. The actual ORF can be quickly

calculated in a loop over frequencies from the seed matrices. This method of calculating the ORF is the fastest with reasonable memory usage.

To calculate the ORF in the SpH basis we used the existing `PyStoch` module of calculating ORF in the pixel basis and then converting them in the SpH basis using `HEALPix` tools. This method is extremely fast and accurate and does not require dealing with SpH formulas (`HEALPix` tools do that internally). However, the regular `HEALPix` tools for calculating SpH maps from pixel maps work for real maps only, so we had to wrap that routine into a new one to handle complex ORF maps.

After performing the basis conversion of ORF for the first time segment, calculating the ORF for other time segments can be made faster by exploiting the earth rotation time-dependency given in Eq. (10). This way by using ORF seed matrices and azimuthal symmetry, the ORF in the SpH basis can be calculated very accurately and very quickly even for very high l_{max} (see Fig.3). This unification of techniques from the two methods enables us to efficiently create maps in both pixel and SpH bases.

B. Calculating dirty map

Starting from Eq. (5), the expression of the dirty map can be simplified as,

$$X_p = \sum_{I f_{ts}} K_{f_{ts}, p}^{I*} x_{f_{ts}}^I, \quad (14)$$

where $K_{f_{ts}, p}^I := \tau H(f) \gamma_{f_{ts}, p}^I$ is the mapping kernel and $x_{f_{ts}}^I$ is folded time frequency data [23] which is calculated from the CSD $\tilde{s}_{\mathcal{I}_1}^*(t; f) \tilde{s}_{\mathcal{I}_2}(t; f)$. The calculation of the dirty map is straightforward once the ORF has been calculated. Just by changing the basis of the ORF from pixel to SpH, the basis of the resulting dirty map changes without requiring any modification in the `PyStoch` algorithm.

Previously we noted and demonstrated that calculation of SGWB skymaps can be done in a few minutes on an ordinary laptop [24]. The SpH search we present here is not only an order of magnitude faster than the conventional SpH search owing to folded data and the way it is handled by `PyStoch`, it is even faster than the `PyStoch` pixel search because the SpH maps have fewer terms compared to the pixel maps (961 for $l_{\text{max}} = 30$ compared to 3072 pixels).

In order to make sure that the enhanced `PyStoch` pipeline with unified map-making capability produces similar results with the one used in [26, 27], we did some investigation on the dirty maps obtained from the new pipeline and the conventional one [30]. In Fig. 4, we show the dirty maps obtained from the two pipelines. To further demonstrate the validity of the upgraded `PyStoch`, we compared the spherical harmonic coefficients obtained from these two different methods in Fig. 5. It is evident that the obtained results are identical, validating

¹ For illustration purposes we set $n_{\text{side}} = 32$ in all the skymaps

² Here, l_{max} is chosen somewhat arbitrarily and the choice is consistent with previous LVC stochastic studies.

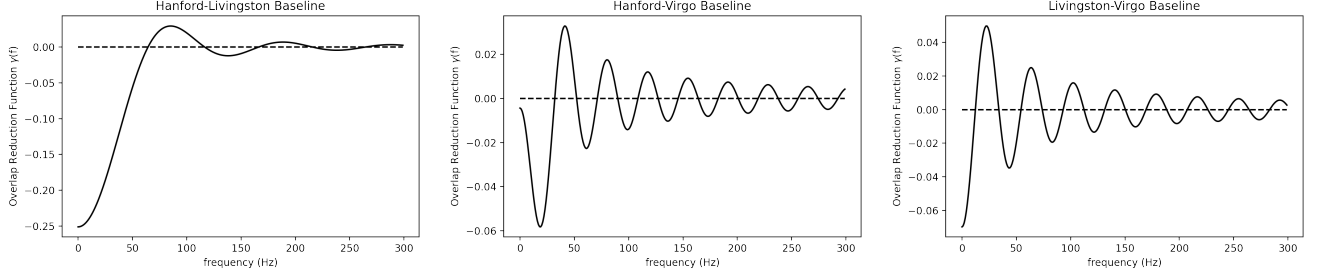


FIG. 3. The first spherical harmonic term in the overlap reduction function as calculated by enhanced **PyStoch** for the three possible baselines in LIGO Virgo detector network. The solid line is for the real part of the function, dashed line is complex.

the dirty map-making part of our pipeline.

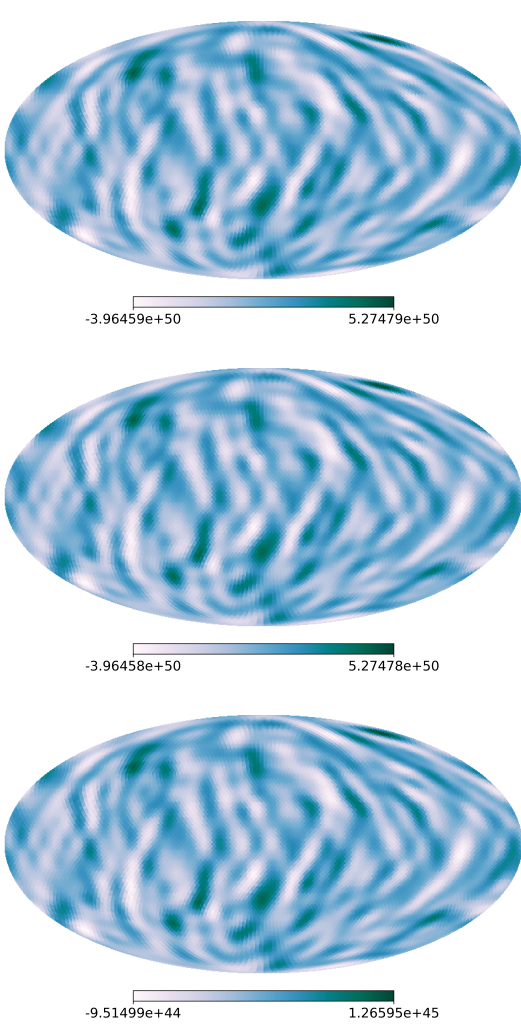


FIG. 4. Dirty maps produced using the conventional pipeline is given on the top whereas the one from **PyStoch** pipeline is at the middle. On the bottom, we showed the difference between the dirty maps. The RMS difference of these maps are of the order of few times 10^{-5} . All the maps have been produced with $n_{\text{side}} = 32$, power-law spectral indices $\alpha = 3$ and have $l_{\text{max}} = 30$.

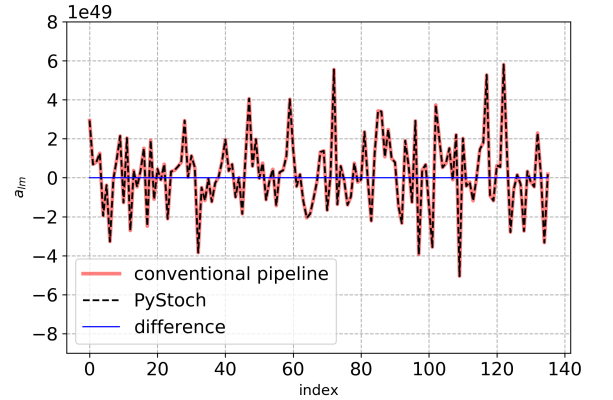


FIG. 5. Spherical harmonic coefficients, a_{lm} computed from two different methods. Here we restrict the results up to $l_{\text{max}} = 15$, corresponding to 256 total modes. The thick solid line represents a_{lm} computed using the conventional pipeline whereas the black dashed line is obtained using **PyStoch**. The differences in their values, showed with a thin solid line, are nearly zero. An RMS difference of few times 10^{-5} (as was the case for dirty maps in Fig. 4) validates the SpH coefficients as well as the dirty map computed using the new pipeline.

C. Calculating Fisher information matrix

The “clean” map is obtained by numerically deconvolving the beam function from the dirty map. This deconvolution process requires the calculation of beam function at every point on the sky, which can be understood as equivalent to making one dirty map for each pixel by placing a unit point source at that pixel. Even though the computational cost of this calculation scales as the square of number of pixels, using the algebraic method proposed in [24] we were able to calculate them for our analysis. The challenge to obtain the Fisher matrix in the SpH basis becomes trivial, given we have now calculated the ORF and dirty maps in the SpH basis. Following the recipe from Sec. II, we have successfully calculated

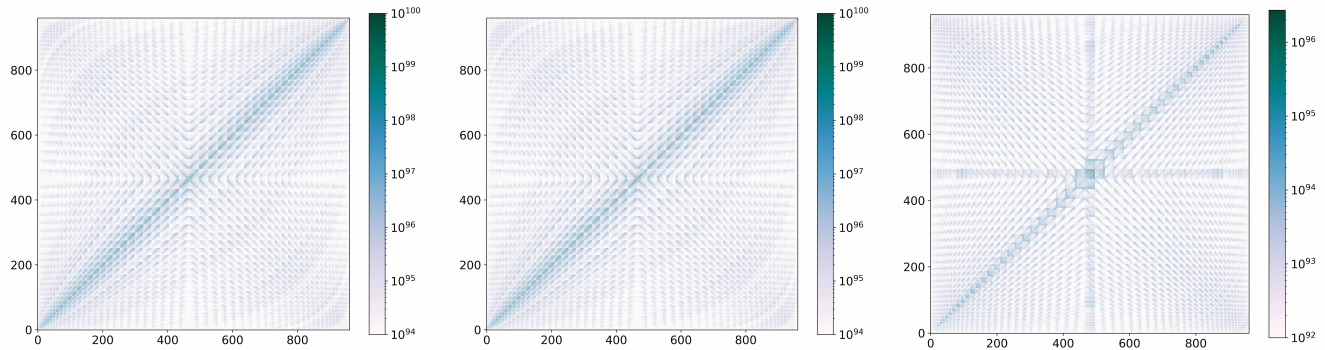


FIG. 6. Fisher matrix (absolute value) produced using the conventional pipeline is shown on the left whereas the one from **PyStoch** is in the middle. On the right, we show the absolute difference between the Fisher matrices, whose small values validate the consistency between the pipelines (elements with too small absolute differences have been masked to avoid the divergence of the log of a value close to zero). From the RMS difference of these matrices, the agreement can be quantified to be better than one part in 10^4 . Here the power-law spectral index and l_{\max} take the same values as of the dirty maps in Fig. 4.

this matrix. In Fig. 6, we present the Fisher information matrix calculated using the conventional pipeline and **PyStoch**. From this figure, it is evident the results are the same. One can now use this Fisher matrix to obtain the clean map and the corresponding angular scale of the structure found in the map.

The Fisher (beam) matrix for a single baseline of two detectors has poorly observed modes, which makes direct inversion of the Fisher matrix (Fig. II,6), impractical. ML estimation of the true SGWB sky takes the simple form given in Eq. (4), only when the inverse of the beam matrix exists. To obtain the true SGWB sky, one has to deconvolve the dirty maps either by linearly solving the convolution equation [20] or by applying appropriate regularization in Γ before the inversion [31]. **PyStoch** is capable of handling any standard regularisation (norm-regularisation, gradient regularisation, Singular Value Decomposition (SVD), etc.) to condition the Fisher matrix $\Gamma'_{lm,l'm'}$. Though comparing the relative performances of these deconvolution schemes in the analysis of present data is outside the scope of this paper, we have illustrated this procedure for SVD regularization case in Appendix A.

IV. CONCLUSIONS

The implementation of the SpH search in **PyStoch** has unified and streamlined the different kinds of stochastic searches in an unprecedented way. Previously the standard pipeline used to produce SpH and pixel maps without a proper scope for comparing and validating the results while maintaining statistical accuracy. Now we incorporate a proper basis transformation using the mathematical symmetries of past formalisms. We validated that this basis transformation works accurately for the

maps and the Fisher matrices. From now on multiple SGWB maps need not be produced from the data. The tools we incorporated in **PyStoch** will be sufficient to perform the standard SpH analysis on the latest dataset. Another example of how multiple searches have been united would be to consider the isotropic search. One only needs to run **PyStoch** in SpH basis with $l_{\max} = 0$. We can get the isotropic search results at every frequency as well as for the broadband analyses.

Even though in this paper we have restricted to one spectral shape of the modeled power spectral density of the source, it has been shown previously that the analysis using **PyStoch** mitigates the need to perform separate searches for different spectral shapes. Since these properties are preserved in the enhanced **PyStoch**, one can trivially perform a model-independent mapping of the SGWB sky.

Thus, **PyStoch** is now ready to perform any 2-sphere analysis to search for SGWB anisotropy (narrowband, or broadband) the literature has to offer. SGWB results, although not impressive in spatial resolution, are complex in structure. It has incredible cosmological and astrophysical information hidden in it. A lot of studies e.g. lensing, multi-point correlation, polarization remain to be performed on them. Our effort of unifying the preliminary analysis of SGWB provides a robust launchpad for future studies.

ACKNOWLEDGMENTS

The authors thank Joe Romano for carefully reading the manuscript and providing valuable comments. This work significantly benefitted from the interactions with the Stochastic Working Group of the LIGO-Virgo-KAGRA Scientific Collaboration. We acknowledge the

use of IUCAA LDAS cluster Sarathi for the computational/numerical work. JS acknowledges the support by JSPS KAKENHI Grant Number JP17H06361 and expresses thanks to Hideyuki Tagoshi and Hirotaka Yuzurihara for the helpful discussion. AA acknowledges support by INFN Pisa and EGO and wants to thank Giancarlo Cella for his support. SM acknowledges support from the Department of Science and Technology (DST), India, provided under the Swarna Jayanti Fellowships scheme. This article has a LIGO document number LIGO-P2000461.

Appendix A: SVD regularization and C_l estimates

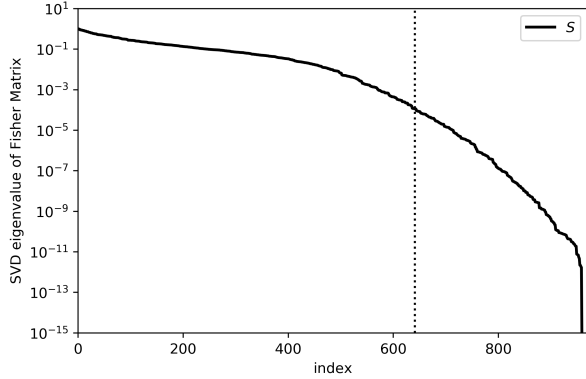


FIG. 7. SVD eigenvalues of the Fisher information matrix $\Gamma_{lm,l'm'}$ is represented using the solid line. The dotted vertical line demarcates the eigenvalues considered for the inversion of regularized Fisher matrix $\Gamma'_{lm,l'm'}$. For demonstration, we have considered $l_{\max} = 30$ (961 modes).

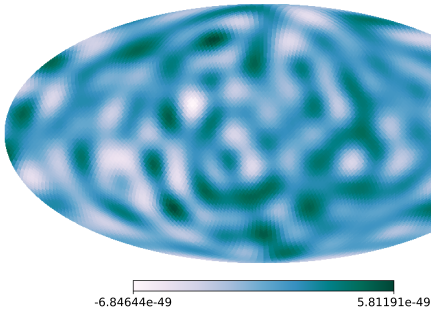


FIG. 8. Clean map produced using the SVD regularized Fisher matrix. These maps are obtained for a power-law spectral indices $\alpha = 3$ and contains information up to $l_{\max} = 15$.

Earlier studies utilized the singular value decomposition (SVD) techniques to characterise [20] and to condition [13, 21] the Fisher matrix. In this paper, as an example, we use the SVD technique to obtain the clean maps, even though PyStoch is capable of handling any type of regularized deconvolution [31]. The Fisher ma-

trix, from its definition in Eq. (6) is Hermitian, so its SVD takes the form,

$$\Gamma = USU^*, \quad (\text{A1})$$

where U is a unitary matrix and S is a diagonal matrix, whose non-zero elements are the positive and real eigenvalues of the Fisher matrix, arranged in descending order. To condition the matrix, a threshold S_{\min} is chosen. The choice is made by considering the proper trade-off between the quality of the deconvolution and the increase in numerical noise from less sensitive modes. Any values below this cut-off are considered too small and we replace them with infinity. Alternatively, they can be replaced with the smallest eigenvalue above the cut-off. In this demonstration, the singular value cutoff is chosen as 10^{-3} of the maximum eigenvalue. Any value below this threshold is padded by the S_{\min} .

Now, one can easily write the inverse of regularized Fisher matrix, which is obtained using the modified S' (see Fig. 7) as,

$$\Gamma'^{-1} = US'^{-1}U^*. \quad (\text{A2})$$

By multiplying the inverted-regularised Fisher matrix with the dirty map, one can obtain the estimators of the spherical harmonic coefficients,

$$\hat{\mathcal{P}}_{lm} = \Gamma'^{-1}_{lm} X_{lm}. \quad (\text{A3})$$

One can use the above clean map (Fig.8) in the SpH basis, to construct the unbiased estimator of the angular power spectra, i.e.,

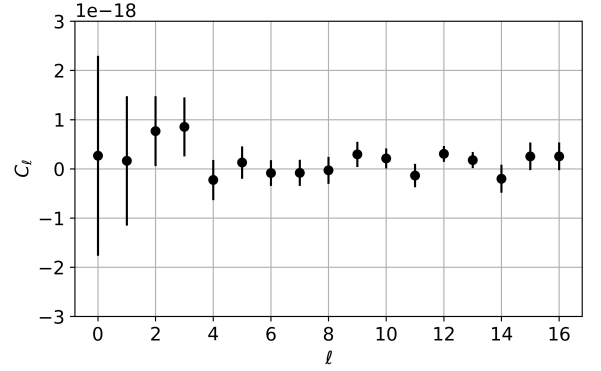


FIG. 9. Estimate of the angular power spectrum, C_l , of the SGWB for a spectral shape characterized by $\alpha = 3$.

$$\hat{C}_l = \frac{1}{2l+1} \sum_m \left[|\hat{\mathcal{P}}_{lm}|^2 - (\Gamma'^{-1})_{lm,lm} \right]. \quad (\text{A4})$$

We have also computed the estimate of the angular power spectrum, C_l (describes angular scale of the structure found in the clean map), of the SGWB for a specific spectral distribution or signal model. Fig. 9 shows the obtained C_l characterized by spectral index, $\alpha = 3$ from the folded data set.

-
- [1] B. Abbott *et al.* (LIGO Scientific, Virgo), Phys. Rev. Lett. **116**, 061102 (2016), arXiv:1602.03837 [gr-qc].
 - [2] R. Abbott *et al.* (LIGO Scientific, Virgo), (2020), arXiv:2010.14527 [gr-qc].
 - [3] B. Allen, in *Relativistic Gravitation and Gravitational Radiation*, edited by J.-A. Marck and J.-P. Lasota (1997) p. 373, gr-qc/9604033.
 - [4] B. Allen and A. C. Ottewill, Phys. Rev. D **56**, 545 (1997).
 - [5] B. P. Abbott, R. Abbott, T. D. Abbott, F. Acernese, K. Ackley, C. Adams, T. Adams, P. Addesso, R. X. Adhikari, V. B. Adya, and et al., Physical Review Letters **120**, 091101 (2018), arXiv:1710.05837 [gr-qc].
 - [6] S. Dhurandhar, H. Tagoshi, Y. Okada, N. Kanda, and H. Takahashi, Phys. Rev. D **84**, 083007 (2011), arXiv:1105.5842 [gr-qc].
 - [7] S. A. Hughes, Physics of the Dark Universe **4**, 86 (2014), dARK TAUP2013.
 - [8] G. Cusin, R. Durrer, and P. G. Ferreira, Phys. Rev. D **99**, 023534 (2019), arXiv:1807.10620 [astro-ph.CO].
 - [9] C. M. F. Mingarelli, T. Sidery, I. Mandel, and A. Vecchio, Phys. Rev. D **88**, 062005 (2013).
 - [10] N. Mazumder, S. Mitra, and S. Dhurandhar, Phys. Rev. D **89**, 084076 (2014), arXiv:1401.5898 [gr-qc].
 - [11] Z. Arzoumanian *et al.* (NANOGrAV), Astrophys. J. **859**, 47 (2018), arXiv:1801.02617 [astro-ph.HE].
 - [12] L. Bian, J. Liu, and R. Zhou, (2020), arXiv:2009.13893 [astro-ph.CO].
 - [13] J. D. Romano and N. J. Cornish, Living Rev. Rel. **20**, 2 (2017), arXiv:1608.06889 [gr-qc].
 - [14] P. F. Michelson, Monthly Notices of the Royal Astronomical Society **227**, 933 (1987).
 - [15] N. Christensen, Phys. Rev. D **46**, 5250 (1992).
 - [16] E. E. Flanagan, Phys. Rev. D **48**, 2389 (1993).
 - [17] B. Allen and J. D. Romano, Physical Review **D59**, 102001 (1999), gr-qc/9710117.
 - [18] A. Lazzarini and J. Romano, *Use of overlapping windows in the stochastic background search*, Internal working note LIGO-T040089-00-Z (Laser Interferometer Gravitational Wave Observatory (LIGO), 2004).
 - [19] S. W. Ballmer, Class. Quant. Grav. **23**, S179 (2006), arXiv:gr-qc/0510096 [gr-qc].
 - [20] S. Mitra, S. Dhurandhar, T. Souradeep, A. Lazzarini, V. Mandic, *et al.*, Phys. Rev. **D77**, 042002 (2008), arXiv:0708.2728 [gr-qc].
 - [21] E. Thrane, S. Ballmer, J. D. Romano, S. Mitra, D. Talukder, S. Bose, and V. Mandic, Phys. Rev. **D80**, 122002 (2009), arXiv:0910.0858 [astro-ph.IM].
 - [22] A. I. Renzini and C. R. Contaldi, Phys. Rev. D **100**, 063527 (2019).
 - [23] A. Ain, P. Dalvi, and S. Mitra, Phys. Rev. **D92**, 022003 (2015), arXiv:1504.01714 [gr-qc].
 - [24] A. Ain, J. Suresh, and S. Mitra, Phys. Rev. **D98**, 024001 (2018), arXiv:1803.08285 [gr-qc].
 - [25] K. M. Gorski, E. Hivon, A. J. Banday, B. D. Wandelt, F. K. Hansen, M. Reinecke, and M. Bartelman, Astrophys. J. **622**, 759 (2005), arXiv:astro-ph/0409513 [astro-ph].
 - [26] B. P. Abbott *et al.* (LIGO Scientific, Virgo), Phys. Rev. Lett. **118**, 121102 (2017), arXiv:1612.02030 [gr-qc].
 - [27] B. Abbott *et al.* (LIGO Scientific, Virgo), Phys. Rev. D **100**, 062001 (2019), arXiv:1903.08844 [gr-qc].
 - [28] J. D. Jackson, *Classical Electrodynamics* (Wiley, 1998).
 - [29] L. S. Finn, S. L. Larson, and J. D. Romano, Phys. Rev. **D79**, 062003 (2009), arXiv:0811.3582 [gr-qc].
 - [30] <https://git.ligo.org/stochastic-public/stochastic>.
 - [31] S. Panda, S. Bhagwat, J. Suresh, and S. Mitra, Phys. Rev. D **100**, 043541 (2019).